Facile Preparation of Commercial Bi_2O_3 Nanoparticle Decorated Activated Carbon for Pseudocapacitive Supercapacitor Applications

Osman Üner
Kırklareli Üniversitesi: Kirklareli Universitesi
Naim Aslan
Munzur Universitesi
Akın Sarıoğlu
Kırklareli Üniversitesi: Kirklareli Universitesi
Fatih Semerci
Kırklareli Üniversitesi: Kirklareli Universitesi
Mumin Mehmet Koc (mumin.koc@port.ac.uk)
Kirklareli Universitesi https://orcid.org/0000-0003-4500-0373

Research Article

Keywords: Supercapacitor, Inorganic-organic composite, Bismuth Oxide

Posted Date: March 17th, 2021

DOI: https://doi.org/10.21203/rs.3.rs-300598/v1

Abstract

In this work, a facile method to prepare commercial nano-Bi_2O_3/carbon composites with high pseudocapacitive properties was presented. The inorganic-organic composites synthesized by using commercial bismuth oxide and active carbon with different weight ratio. The composites were characterized using microscopic, spectroscopic, and diffractive methods. Our assessments confirmed that active carbons were successfully doped with commercial Bi_2O_3 nanoparticles with different dopant rates. The composites exhibited a maximum specific capacitance of 517 F/g at a current density of 1 A/g for 20% Bi_2O_3 nanoparticle doped activated carbon samples. Augmented discharging time was also achieved for increased Bi_2O_3 nanoparticle doping rate. Increased Bi_2O_3 dopant rate also increased the calculated specific capacitance.

1. Introduction

Renewable energy sources have attracted great attention to meet the increasing energy needs [1–5]. However, the majority of renewable energy sources such as wind and solar energy have an intermittent nature, which is ideally to be stored in devices [6]. As an electrochemical energy-storage devices supercapacitor attracted attention for several reasons such as their relatively high-power densities and energy densities compared to most of batteries and conventional capacitors [7–9]. Charge storage mechanism of supercapacitors can be classified as electrochemical double layer capacitors (EDLCs) and pseudocapacitors [10]. EDLCs store charges by electrostatic charge separation on the surface of the materials, whereas pseudocapacitors are based on a redox reaction process [11]. Pseudocapacitors provide a supercapacitor with higher specific capacitances and energy densities than EDLCs [12]. Activated carbons have displayed great potential as efficient electrodes for EDLC type supercapacitors due to high micro/mesoporousity, their high specific unique pore structure for efficient ion diffusion and low cost [13]. Although porous activated carbon (AC) as a supercapacitor has a high-power density and a long cycle life it has relatively low specific capacitance [14]. Heteroatoms in the porous carbon networks improve surface wettability of the electrode and contribute additional pseudo-capacitance to the total capacitance in the active carbon derivatives [14–16].

Owing to their large capacitance and high energy density as a result of reversible redox reactions different pseudocapacitive materials were designed extensively as electrode materials for supercapacitors such as metal oxides, metal sulphides and metal selenides [17].

Nanoparticles illustrate outstanding electrical, electronical, optical and magnetic properties with good electron affinity [18–20]. Metal oxides nanoparticles such as Co_3O_4 and NiO are also considered pseudocapacitive electrodes in aqueous electrolytes [9, 21–23]. They are also researched extensively in batteries as electrode active materials [24]. Among the pseudocapacitive materials for supercapacitors, bismuth oxide has been largely investigated because of its good electrochemical properties, stabilities and relatively high power [25–29]. As a result, the fabrication of active carbon composites with

pseudocapacitive materials is a very effective method to enhance the specific capacitance of supercapacitors [30, 31].

In this work, we report a facile method to synthesize a nanocomposite from commercial bismuth oxide and plant based activated carbon materials for supercapacitor applications. The composite was characterized by PXRD (powder x-ray diffraction), FE-SEM (field emission scanning electron microscope), FTIR (Fourier transform infrared spectra), thermogravimetric analysis. The electrochemical properties of the nanocomposites were measured in 6 M KOH electrolyte by using a three-electrode system. The as-prepared samples show a maximum specific capacitance of 565 F/g at a current density of 1 A/g.

2. Experimental

2.1. Measurements and materials

All starting materials were of analytical reagent grade and used as received without further purification. SETARAM LABSYS evo TG/DTA thermal analyser was used to record simultaneous TG, DTG and DTA curves in the dry air atmosphere at a heating rate of 10 ºC min^{-1} in the temperature range 30–800 ºC using alumina crucibles. JASCO FTIR-6700 spectrum was used in the FTIR assessments in the range between 400 and 4000 cm^{-1}.

2.2. Electrode Preparation for Electrochemical Measurements

The commercial Bi_2O_3-Active Carbon composite (75%) and acetylene black (15%) were ground and mixed in an agar mortar for 30 min. Then, PVDF (10%) was added to mortar, and the resultant mixture was again ground for 15 min. A few drops of N-methylpyrrolidone were added to the slurry mixture. The mixture was then dropped onto Ni foam (10 X 10 cm), dried in an oven at 60°C for 24 h and pressed at a pressure of 5 MPa. Finally, the obtained electrode was left to soak in 6 M KOH solution for overnight.

2.3. Characterization

Cyclic voltammetry (CV), chronopotansiyometry (CP) and electrochemical impedance spectroscopy techniques (EIS) were used to characterize the electrochemical capacitance properties of the nanomaterials using a Gamry Reference 600 potentiostat/galvanostat/ZRA. The frequency limits were typically set between 5 mHz and 100 kHz. The AC oscillation amplitude was 5 mA under an open-circuit potential.

2.3. Preparation of Composites

As given in the paper of Üner and coworkers in 2021, the activated carbon obtained with the highest surface area from ripe black locust seed pods was used in this study, and also detail information about the synthesis, optimization and characterization of this activated carbon can be reached from this published paper [32]. To synthesize 10%-Bi_2O_3@AC and 20%-Bi_2O_3@AC, 0.1 and 0.2 g Bi_2O_3 were

dissolved by using 200 mL distilled water separately in 250 mL Erlenmeyer flasks. For better dissolution of Bi_2O_3, the Erlenmeyer flasks were put in ultrasonic water bath (isolab laborgerate GMBH) and hold for 20 minutes. Then, 1 g activated carbon was added into each Erlenmeyer flask, and stirred at 150 rpm for 72 hours by using a magnetic stirrer (Phoenix stir RSM-03-10KH). After that, these aqueous 10% and 20% Bi_2O_3@AC mixtures in Erlenmeyer flasks were filtered, washed with distilled water, and dried at 50°C in an incubator (Termal Lab). The obtained 10%-Bi_2O_3@AC and 20%-Bi_2O_3@AC were stored in lidded glass bottles for further experiments and analyses.

3. Results And Discussion

3.1. Structural Characterization

SEM, EDX, EDX mapping, FTIR and XRD methods were used in the structural characterization. Figure 1 illustrates SEM characteristics of pure Bi_2O_3 nanoparticles, pure activated carbon, Bi_2O_3 nanoparticle doped activated carbon structures. Figures confirm that Bi_2O_3 structures are in nanoparticle form which are in grainy structure the size of nanoparticles were found to be approx. 100–200 nm. Activated carbon is in robust structure where small carbon particles could be identified. Some pores and flaws can be identified in the SEM image. Doping activated carbon with Bi_2O_3 nanoparticles slightly alters the surface of the activated carbon. In Fig. 1c and 1d, it was seen that small nanoparticles cover the surface of the activated carbon, flake like structures can be also be identified on the surface of the activated carbon.

EDX results of pure Bi_2O_3 nanoparticles, pure activated carbon, Bi_2O_3 nanoparticle doped activated carbon structures were illustrated in Fig. 2. EDX results confirm that Bi_2O_3 nanoparticles and activated carbon is in pure structure where no contamination was seen in the EDX peaks. EDX spectra in Fig. 2 illustrate that decorating activated carbon with Bi_2O_3 nanoparticles were successful, since Bi, O and C peaks can be identified in Fig. 2c and 2d. It was also seen that increased doping rate enhanced the amount of measured Bi in the structure.

Figure 3 illustrates EDX mapping results where EDX maps of pure Bi_2O_3 nanoparticles, pure activated carbon , Bi_2O_3 nanoparticle doped activated carbon structures were illustrated. EDX maps of the samples show no contamination. In Figure 3a, Bi and O structures were seen. In Figure 3b only C and O structures were seen on the surface. In figure 3c, C, O and Bi were seen where oxygen covers almost whole surface, but Bi nanoparticles can also be seen. Figure 4a exhibit similar characteristics to Figure 3a. Surface is mostly covered with oxygen; in addition, Bi and C structures can be identified. Such a map may be an indication of oxidized nanoparticles.

FTIR spectra of pure Bi_2O_3 nanoparticles, pure activated carbon, Bi_2O_3 nanoparticle doped activated carbon structures were presented in Fig. 4. FTIR spectra of samples were given in Fig. 4. Spectra show bands appearing at 1500, 1700, and 3600 cm^{-1} which correspond to the stretching frequencies of oxygen in C = O, aromatic C = C and O-H, respectively. Bi_2O_3 nanoparticle doped activated carbon

structures clearly illustrates that the peaks around 550–560 cm^{-1} are related with metal oxygen bond and 1000 cm^{-1} which corresponds to Bi-O stretching frequencies [33].

Figure 5 illustrates XRD diffraction pattern of nanoparticles and nanocomposites. Two bumps can be seen in the diffraction pattern of activated carbon where no apparent peak was seen, it is possible that activated carbon is in amorphous form or in very bad crystallinity. Therefore, no apparent peak can be observed. Bi_2O_3 nanoparticles shows sharp peaks in their XRD patterns between 25 ˚ and 60 ˚ where characteristics indexed to the tetragonal β-Bi_2O_3 crystal formations in 201, 002, 220, 222, 400, 203, 421 and 402 direction [34]. AC with Bi_2O_3 nanoparticles alters the XRD pattern of AC where Bi_2O_3 related peaks were observed. Bi_2O_3 nanoparticle doped AC samples do not show as sharp peaks as pure Bi_2O_3 nanoparticles. Possibly, doping AC with Bi_2O_3 nanoparticles were shadows the original characteristics of Bi_2O_3 nanoparticles.

3.2. Thermal analysis

To study the experimental Bi_2O_3 content in the composites, thermogravimetric analyses was performed on composites, activated carbon and commercial Bi_2O_3. Activated carbon is stable up to around 500°C and thermal decomposition of activated carbon occur in a single stage and decompose into gas products without remaining any ash. It was determined that commercial Bi_2O_3 does not show any mass loss up to 750°C. Therefore, the amount of Bi_2O_3 in the composites was calculated by considering the remaining mass at 750°C. According to the results, the amounts of Bi_2O_3 in 10%-Bi_2O_3@AC and 20%-Bi_2O_3@AC are 9 and 18%, respectively.

3.3. Electrochemical Measurements

Electrochemical behaviours of Bi_2O_3@AC composites were measured in a three-electrode system in 6 M KOH. It is well-known that the cyclic voltammetry curves of activated carbon-based electrode materials have typically rectangular shape and it indicates that the materials has ideal double-layer capacitance behaviour [35]. In our study, low temperature pyrolyzed of activated carbon exhibits the distinctive redox peaks, that is, while the scan rates are increased, the CV curves turn into fish shape which suggests redox reactions occur onto the activated carbon with 6 M KOH electrolyte (Fig. 2). It might be assumed that the pseudocapacitive behaviour of activated carbon related to faradaic reactions which has plenty of heteroatoms such as nitrogen, oxygen, sulphur on the pore surface of active carbon [15, 36]. The weak peaks at ca. 0.42 and 0.29 V in the CV curve of the activated carbon might be oxidation and reduction reactions of functional groups on the surface of the activated carbon. Also, a small peak at ca. 0.35 V can be seen in CV curves of the Bi_2O_3@AC composites. This may be caused by faradaic reactions of Bi_2O_3. The specific capacitance of the electrodes can be calculated by using cyclic voltammetry according to the following equation [37].

$$C_s = \frac{\int I dV}{vmV} \quad \text{Eq. 1}$$

Where I is the current density (A/cm^2), V is the potential, is the potential scan rate (mV/s) and m (g) is amount of the active material in the composites. The C_s at different scan rates is illustrated in Table 1. Obviously, the Bi_2O_3@AC yields a higher specific capacitance values compared to bare activated carbon electrode (147 F/g at 10 mV/s) at the same scan rates. Furthermore, 20%-Bi_2O_3@AC electrode shows 451 F/g at 10 mV/s while 10%-Bi_2O_3@AC electrode exhibits 285 F/g at the same rate.

On the basis of the cyclic voltammetry analysis, it can be resulted that Bi_2O_3-containing activated carbons show higher specific capacitance values compared to the bare activated carbon. The reason of better electrochemical performance might be ascribed to commercial nano Bi_2O_3 particles effectively reduce the diffusion distance through the charge and discharge processes, the activated carbon exhibits a highly open and irregular micro/meso pore structure that can contribute to the loading of nano Bi_2O_3 particles and lastly pseudocapacitive activated carbon and Bi_2O_3 nanoparticles and have well-matched contact and this is enables transportation of electrons.

Chronopotansiyometry analysis were used to determine the specific capacitance values of the composites. Figure 8 shows the chronopotansiyometry curves of the samples at different current density of 1, 5, 8 and 10 A/g. The shape of the discharge curves suggests the electrodes have pseudocapacitive behaviours. According to the discharge curves of the composites the specific capacitance was calculated by using the following equation [37].

$$C_s = \frac{I \times \Delta t}{m \times \Delta V} \quad \text{(Eq. 2)}$$

Where *I* is the discharge current (A), Δt is the discharge time (s), m is the mass of the loaded active material (g) present in working electrode and is the voltage window (V). Based on the Eq.2, the specific capacitance values of the composites increase with an increase in the discharge time. As shown in Figure 8 (b), 20%-Bi_2O_3@AC shows a much longer discharge time than 10%-Bi_2O_3@AC, which indicates that 20%-Bi_2O_3@AC has a higher specific capacitance. By using Eq. (2) the specific capacitance values for 10%-Bi_2O_3@AC and 20%-Bi_2O_3@AC were calculated and the values are found to be 359 F/g and 565 F/g respectively (Table 2).

The electrochemical impedance measurements were carried out for the as-prepared electrode materials (commercial Bi_2O_3, activated carbon, 10%-Bi_2O_3@AC, and 20%-Bi_2O_3@AC composites). Figure 9 exhibits the Nyquist plots of the electrode materials in 6 M KOH electrolyte in the frequency range of 0.01 to 10^6 Hz. The electrochemically acquired Nyquist plot of the electrodes show the presence of arc-like semi-circle in the high frequency region and a straight line and a short Warburg section between the semicircle and the slope of line. The presence of arc-like semi-circle in the high frequency region suggests that the electrolyte ions interacted well with the electrode material it also represents indication of the conductivity of the electrodes [15, 16, 38]. The charge transfer resistance of the electrodes can be ordered as AC < 20%-Bi_2O_3@AC < 10%-Bi_2O_3@AC < < Bi_2O_3. Besides, the slope of the straight line stands for at an angle of almost 45 exhibits Warburg resistance that points out the ion diffusion resistance of the electrolyte ions

in the electrode material [16]. The ion diffusion resistance of the electrodes can be ordered as Bi_2O_3 < AC < 20%-Bi_2O_3@AC < 10%-Bi_2O_3@AC. The impedance measurements support the cyclic voltammetry and chronopotansiyometry data and the electrochemical properties of the composite electrodes increases with decreasing of the electrochemical resistance.

Table 1
The specific capacitance values from cyclic voltammetry of AC and Bi_2O_3@AC composites

Materials	**Sweep Rates**			
	10 mV/s	25 mV/s	50 mV/s	100 mV/s
AC	147	89	60	40
10%-Bi_2O_3@AC	285	169	114	77
20%-Bi_2O_3@AC	451	272	188	129

Table 2. The specific capacitance values from chronopotentiometry of AC and Bi_2O_3@AC composites

Materials	**Current Densities**			
	1 A/g	5 A/g	8 A/g	10 A/g
AC			47	45
10%-Bi_2O_3@AC	359	224	217	187
20%-Bi_2O_3@AC	565	425	372	337

4. Conclusion

In summary, we have studied a facile method to prepare Bi_2O_3@AC nanocomposites. Experimental methods illustrate that Bi_2O_3 nanoparticles can successfully be doped on activated carbon. Electrochemical properties of nanocomposites were checked. The measurements show that the electrochemical properties of Bi_2O_3@AC composites, which is produced by the synergic contribution of plant based activated carbon and the commercial Bi_2O_3, has the maximum specific capacitance of 20%-Bi_2O_3@AC is about 527 F/g, more than that of activated carbon. The 20%-Bi_2O_3@AC composite would be a potential electrode material for the supercapacitor.

Declarations

Acknowledgements

Part of the project was supported Kirklareli University Scientific Research Coordination Office with project number KLUBAP 207.

References

1. F. Evrendilek, C. Ertekin, Renew. Energy **28**, 2303 (2003)
2. A. Evans, V. Strezov, T.J. Evans, Renew. Sustain. Energy Rev. **16**, 4141 (2012)
3. A. Castillo, D.F. Gayme, Energy Convers. Manag. **87**, 885 (2014)
4. N. Aslan, M.M. Koç, A. Dere, B. Arif, M. Erkovan, A.G. Al-Sehemi, A.A. Al-Ghamdi, F. Yakuphanoglu, J. Mol. Struct. **1155**, 813 (2018)
5. M. Koç, N. Aslan, M. Erkovan, B. Aksakal, O. Uzun, W. Aslam, F. Yakuphanoğlu, Optik (Stuttg). **178**, 316 (2019)
6. J.P. Barton, D.G. Infield, IEEE Trans. Energy Convers. **19**, 441 (2004)
7. L. Zhang, X.S. Zhao, Chem. Soc. Rev. **38**, 2520 (2009)
8. F.E. Atalay, M. Sener, H. Kaya, in *Mater. Today Proc.* (Elsevier Ltd, 2020), pp. 172–179
9. N. Kurnaz Yetim, N. Aslan, A. Sarıoğlu, N. Sarı, M.M. Koç, N.K. Yetim, N. Aslan, A. Sarıoğlu, N. Sarı, M.M. Koç, J. Mater. Sci. Mater. Electron. **31**, 12238 (2020)
10. V. Ruiz, S. Roldán, I. Villar, C. Blanco, R. Santamaría, Electrochim. Acta **95**, 225 (2013)
11. X. Zhao, H. Tian, M. Zhu, K. Tian, J.J. Wang, F. Kang, R.A. Outlaw, J. Power Sources **194**, 1208 (2009)
12. Y. Gogotsi, R.M. Penner, ACS Nano **12**, 2081 (2018)
13. D.S. Su, R. Schlögl, ChemSusChem **3**, 136 (2010)
14. A. Deepi, G. Srikesh, A.S. Nesaraj, Nano-Structures and Nano-Objects **15**, 10 (2018)
15. H. Zhao, B. Xing, C. Zhang, G. Huang, Q. Liu, G. Yi, J. Jia, M. Ma, Z. Chen, C. Zhang, J. Alloys Compd. **766**, 705 (2018)
16. M. Chen, X. Zheng, Y. Ma, X. Dong, Diam. Relat. Mater. **85**, 89 (2018)
17. T. Wang, H.C. Chen, F. Yu, X.S. Zhao, H. Wang, Energy Storage Mater. **16**, 545 (2019)
18. R. Karaçam, N.K. Yetim, M.M. Koç, J. Supercond. Nov. Magn. **33**, 2715 (2020)
19. N. Aslan, B. Ceylan, M.M. Koç, F. Findik, J. Mol. Struct. **1219**, 128599 (2020)
20. N. Kurnaz Yetim, F. Kurşun Baysak, M.M. Koç, D. Nartop, J. Mater. Sci. Mater. Electron. 31, (2020)
21. F.E. Atalay, H. Kaya, D. Asma, A. Bingöl, Biointerface Res. Appl. Chem. **6**, 1099 (2016)
22. F.E. Atalay, E. Yigit, Z.S. Biber, H. Kaya, Nano 13, (2018)
23. N. KURNAZ YETİM, Düzce Üniversitesi Bilim ve Teknol. Derg. 8, 1964 (2020)
24. W.Y. Li, L.N. Xu, J. Chen, Adv. Funct. Mater. **15**, 851 (2005)
25. X. Huang, W. Zhang, Y. Tan, J. Wu, Y. Gao, B. Tang, Ceram. Int. **42**, 2099 (2016)
26. Y. Qiu, H. Fan, X. Chang, H. Dang, Q. Luo, Z. Cheng, Appl. Surf. Sci. **434**, 16 (2018)
27. X.J. Ma, W. Bin Zhang, L. Bin Kong, Y.C. Luo, L. Kang, Electrochim. Acta **192**, 45 (2016)

28. F.L. Zheng, G.R. Li, Y.N. Ou, Z.L. Wang, C.Y. Su, Y.X. Tong, Chem. Commun. **46**, 5021 (2010)
29. N. Kurnaz Yetim, N. Aslan, M.M. Koç, J. Environ. Chem. Eng. 8, (2020)
30. J. Li, Q. Wu, G. Zan, Eur. J. Inorg. Chem. 2015, 5751 (2015)
31. D. Yuan, J. Zeng, N. Kristian, Y. Wang, X. Wang, Electrochem. Commun. **11**, 313 (2009)
32. O. Üner, Ü. Geçgel, and · Tarık Avcu. Carbon Lett. **31**, 75 (2021)
33. A.T. Chipeture, D. Apath, M. Moyo, M. Shumba, J. Anal. Sci. Technol. **10**, 22 (2019)
34. W. Fang, N. Zhang, L. Fan, K. Sun, J. Power Sources **333**, 30 (2016)
35. Y. Wang, Y. Song, Y. Xia, Chem. Soc. Rev. **45**, 5925 (2016)
36. M. Li, C. Liu, H. Cao, H. Zhao, Y. Zhang, Z. Fan, J. Mater. Chem. A **2**, 14844 (2014)
37. J. Yan, T. Wei, B. Shao, Z. Fan, W. Qian, M. Zhang, F. Wei, Carbon N. Y. **48**, 487 (2010)
38. M.C. Liu, L. Bin Kong, P. Zhang, Y.C. Luo, L. Kang, Electrochim. Acta **60**, 443 (2012)

Figures

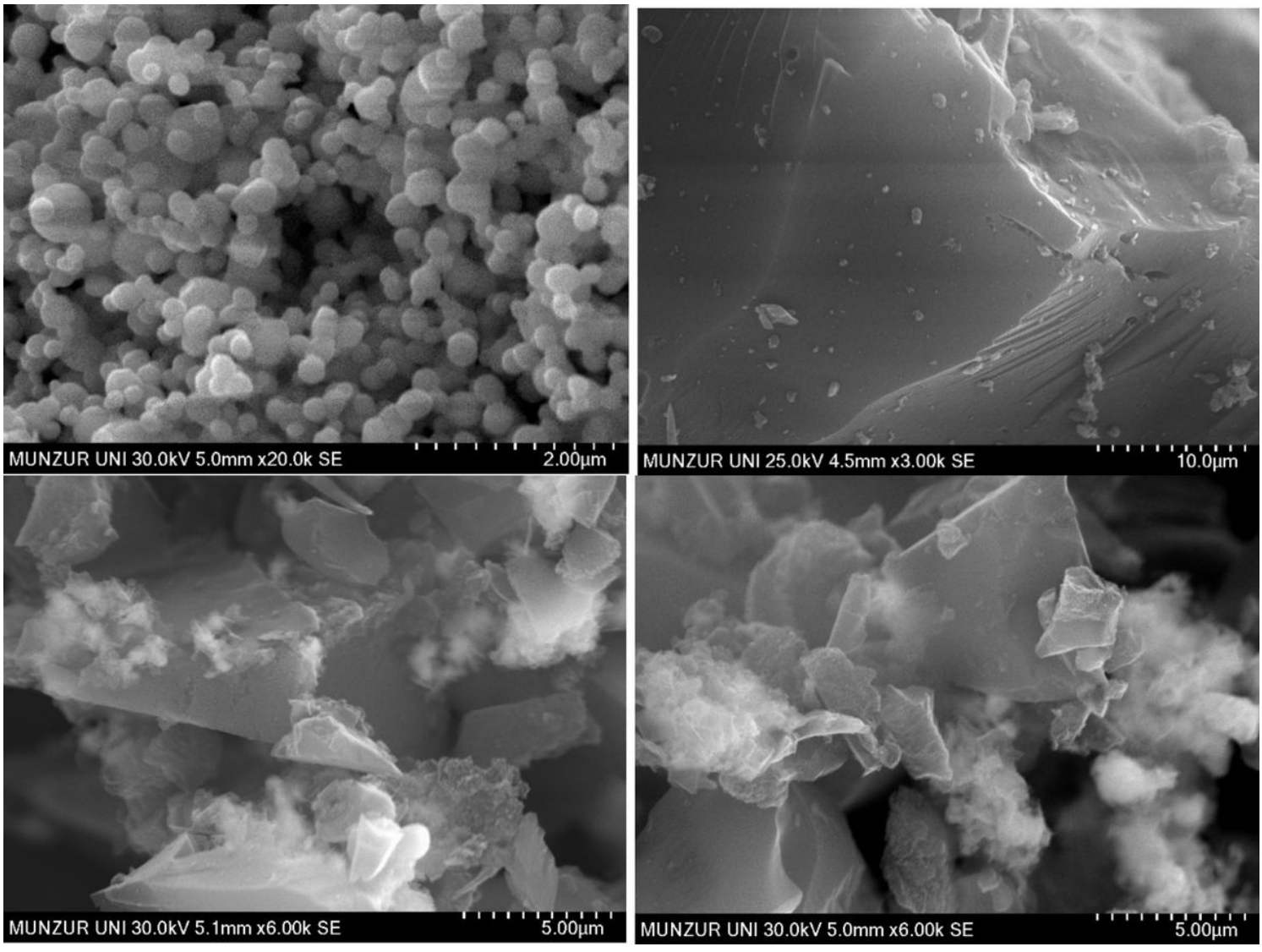

Figure 1

SEM images of pure Bi2O3 nanoparticles (a), pure activated carbon (b), 10% Bi2O3 nanoparticle doped activated carbon (c) and 20% Bi2O3 nanoparticle coated activated carbon.

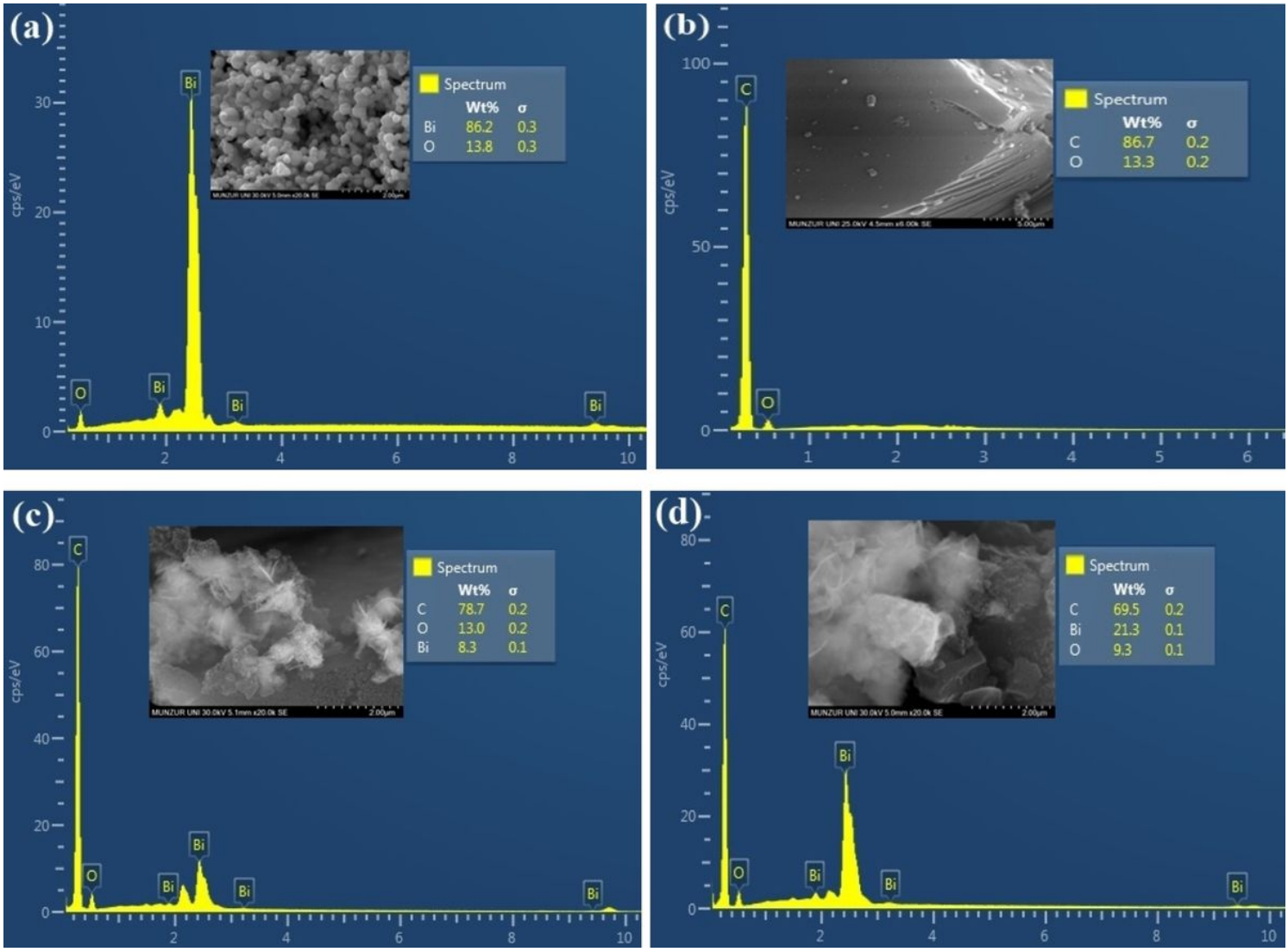

Figure 2

EDX spectra of pure Bi2O3 nanoparticles (a), pure activated carbon (b), 10% Bi2O3 nanoparticle doped activated carbon (c) and 20% Bi2O3 nanoparticle coated activated carbon.

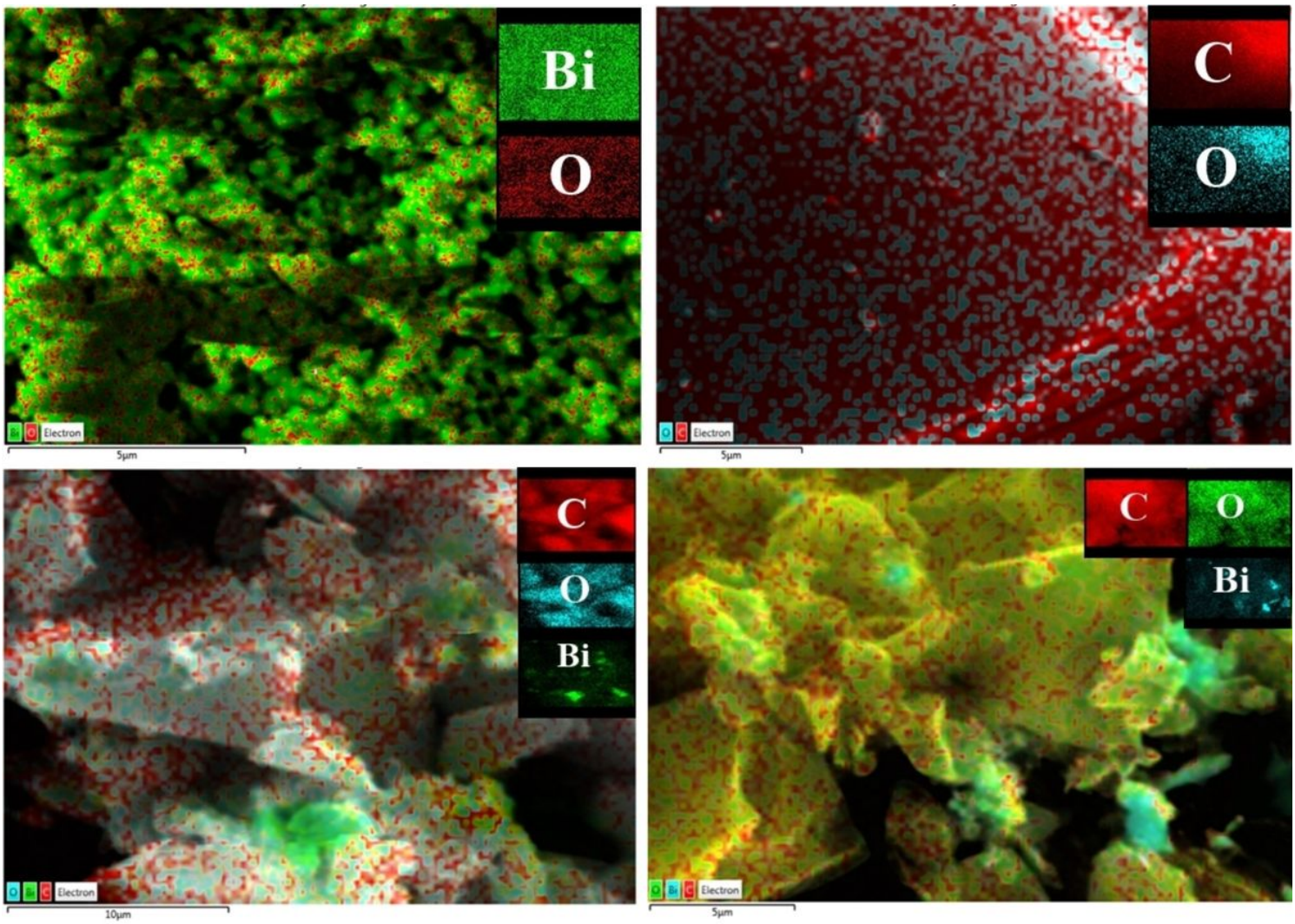

Figure 3

EDX mapping of pure Bi2O3 nanoparticles (a), pure activated carbon (b), 10% Bi2O3 nanoparticle doped activated carbon (c) and 20% Bi2O3 nanoparticle coated activated carbon.

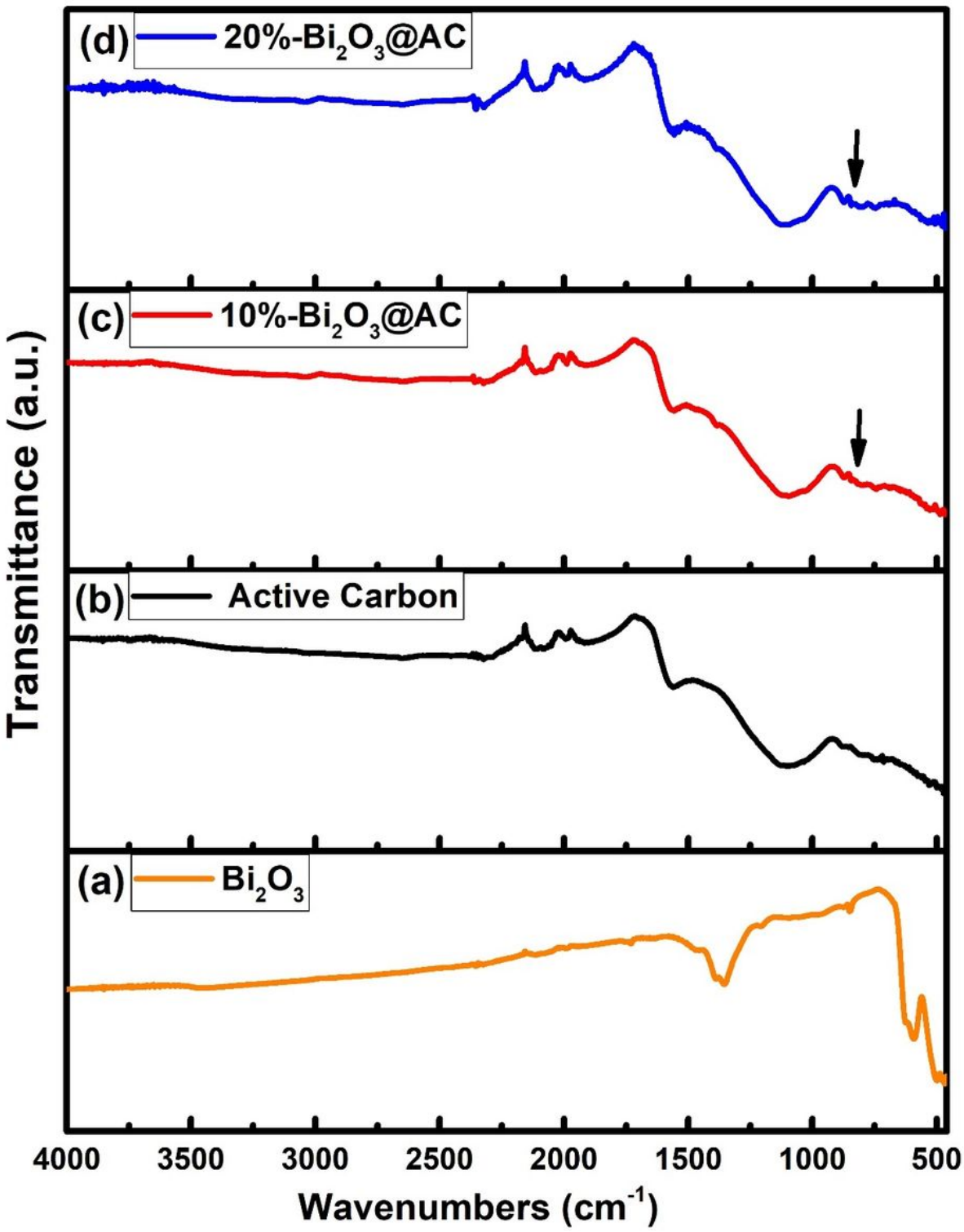

Figure 4

FTIR spectra of pure Bi2O3 nanoparticles (a), pure activated carbon (b), 10% Bi2O3 nanoparticle doped activated carbon (c) and 20% Bi2O3 nanoparticle coated activated carbon.

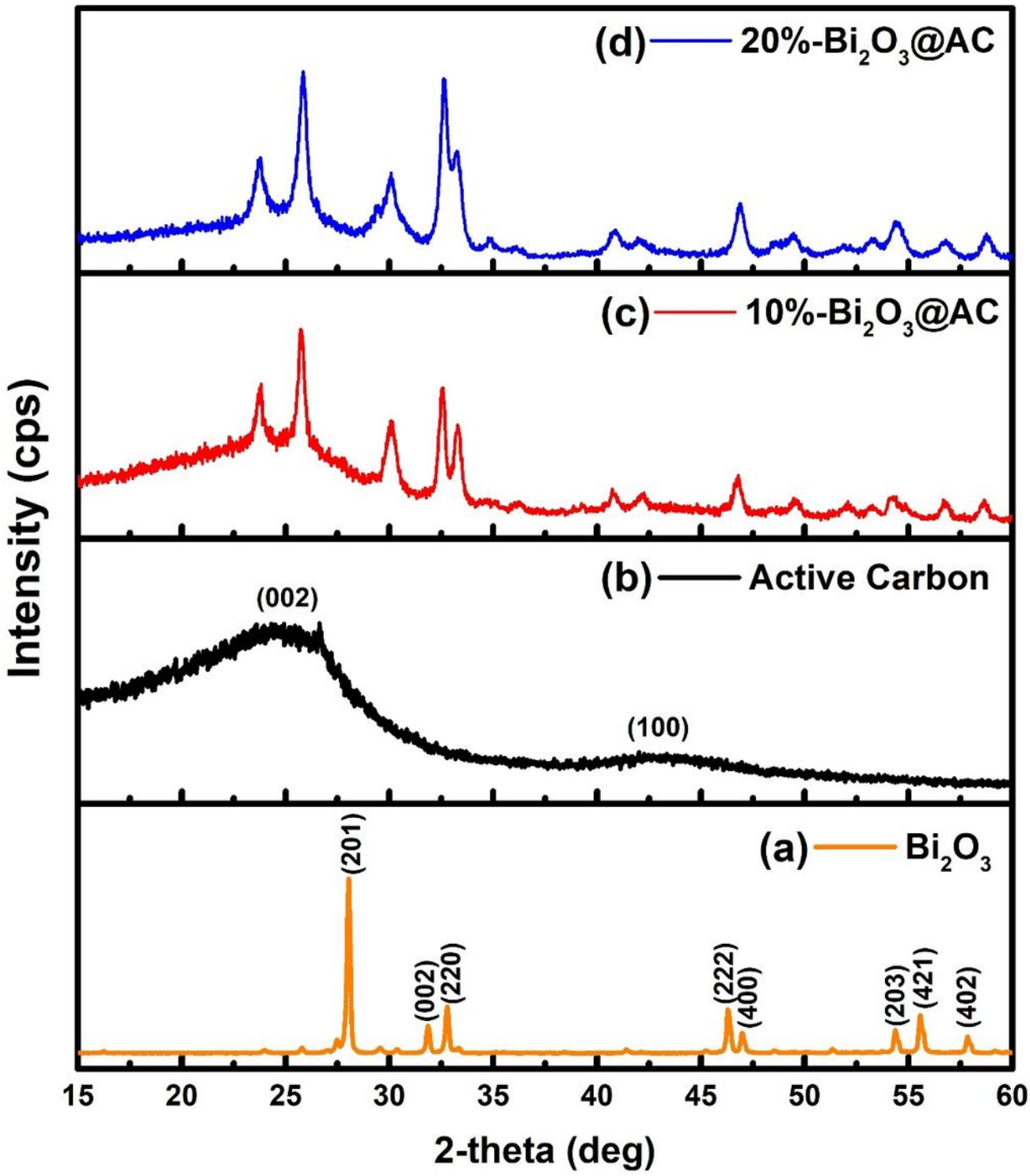

Figure 5

XRD of pure Bi2O3 nanoparticles (a), pure activated carbon (b), 10% Bi2O3 nanoparticle doped activated carbon (c) and 20% Bi2O3 nanoparticle coated activated carbon.

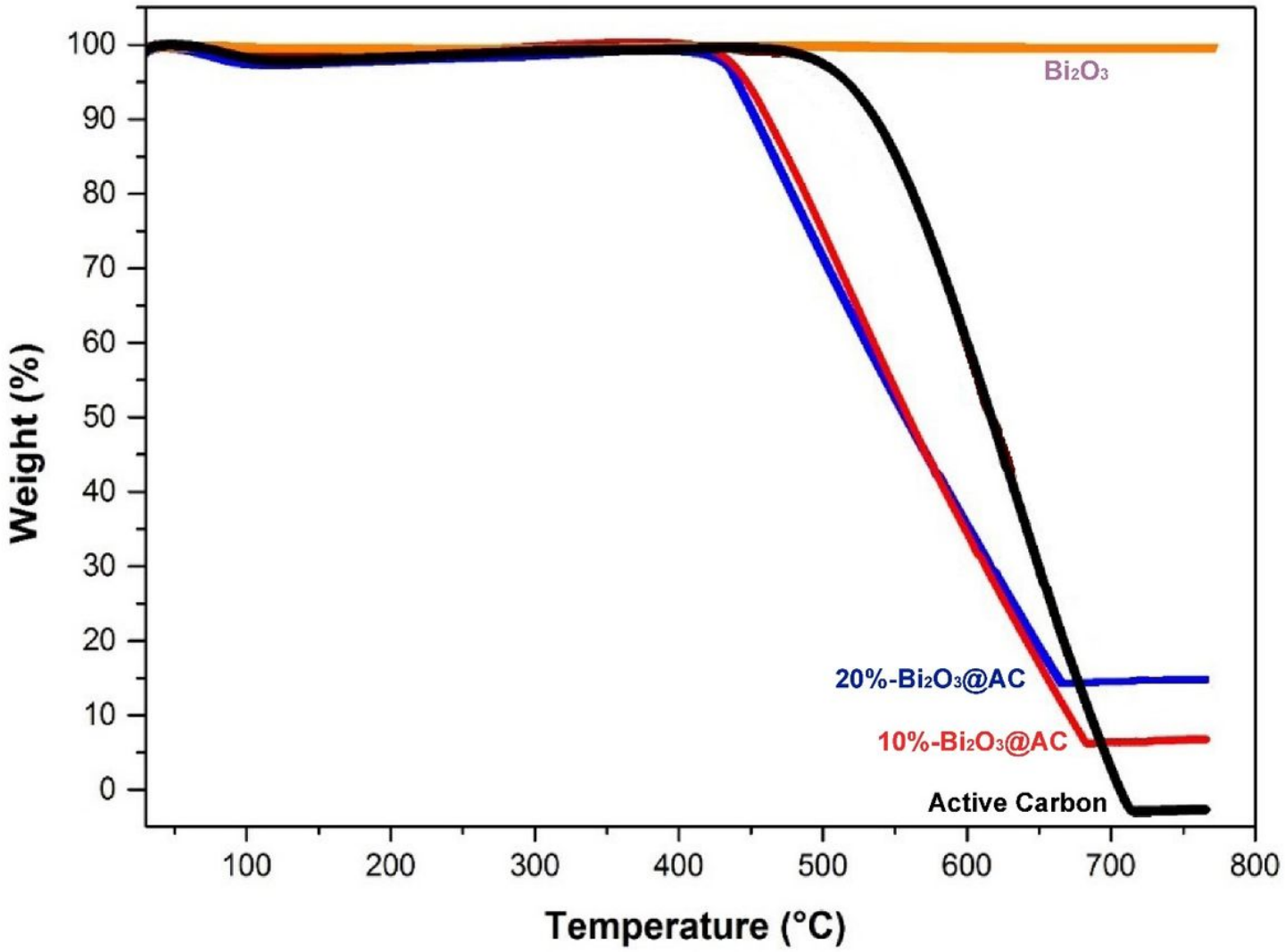

Figure 6

Thermal analysis curves of AC, Bi2O3 and composites

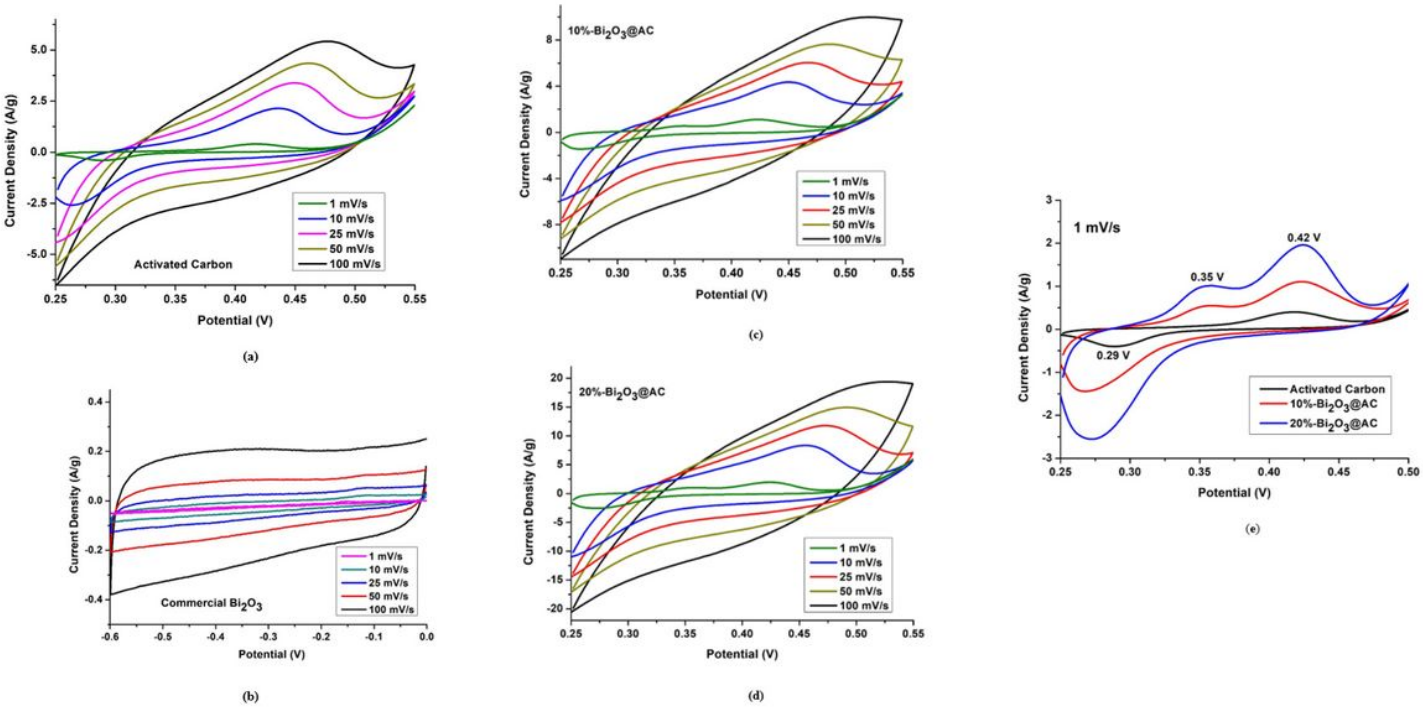

Figure 7

Cyclic voltammograms of (a) activated carbon (b) commercial Bi2O3 (c) 10%Bi2O3@AC (d) 20%Bi2O3@AC at different scan rates and (e) Comparison of materials at 1 mV/s in 6 M KOH electrolyte

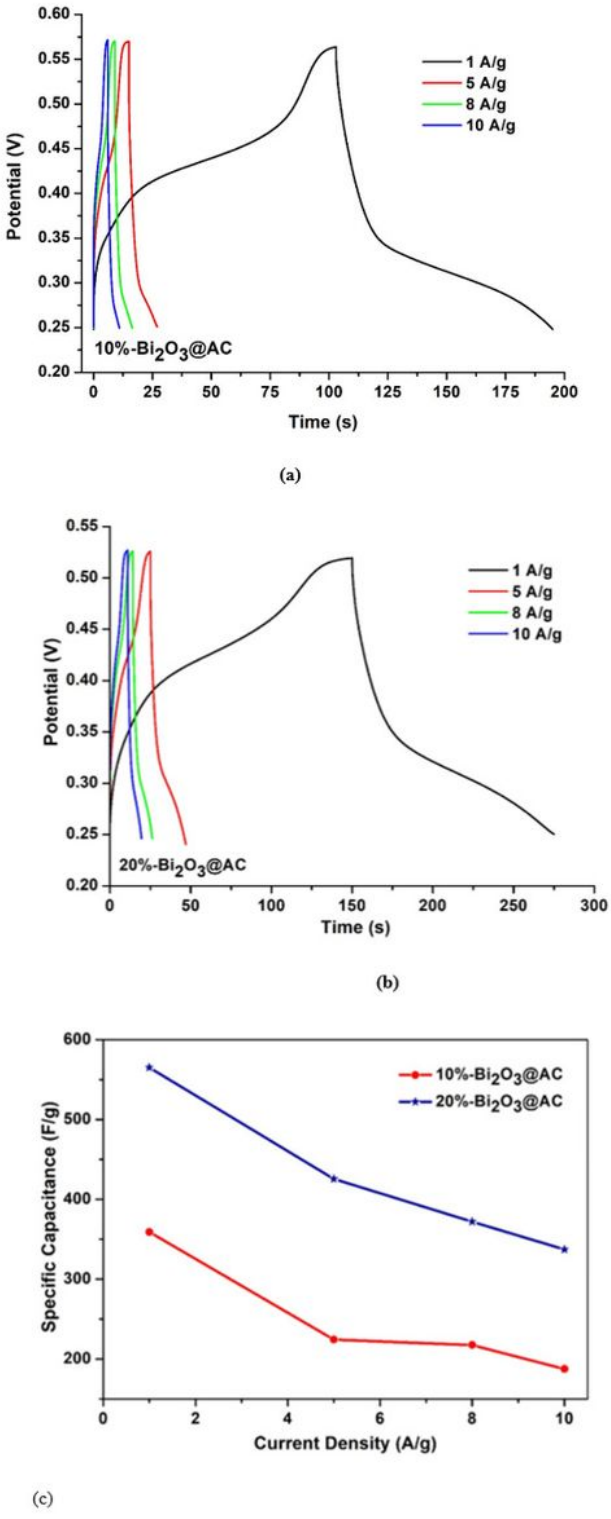

Figure 8

Galvanostatic charge–discharge performance tests for (a) 10%-Bi2O3@AC (b) 20%-Bi2O3@AC (c) rate comparison of the composites at current densities of at different current density

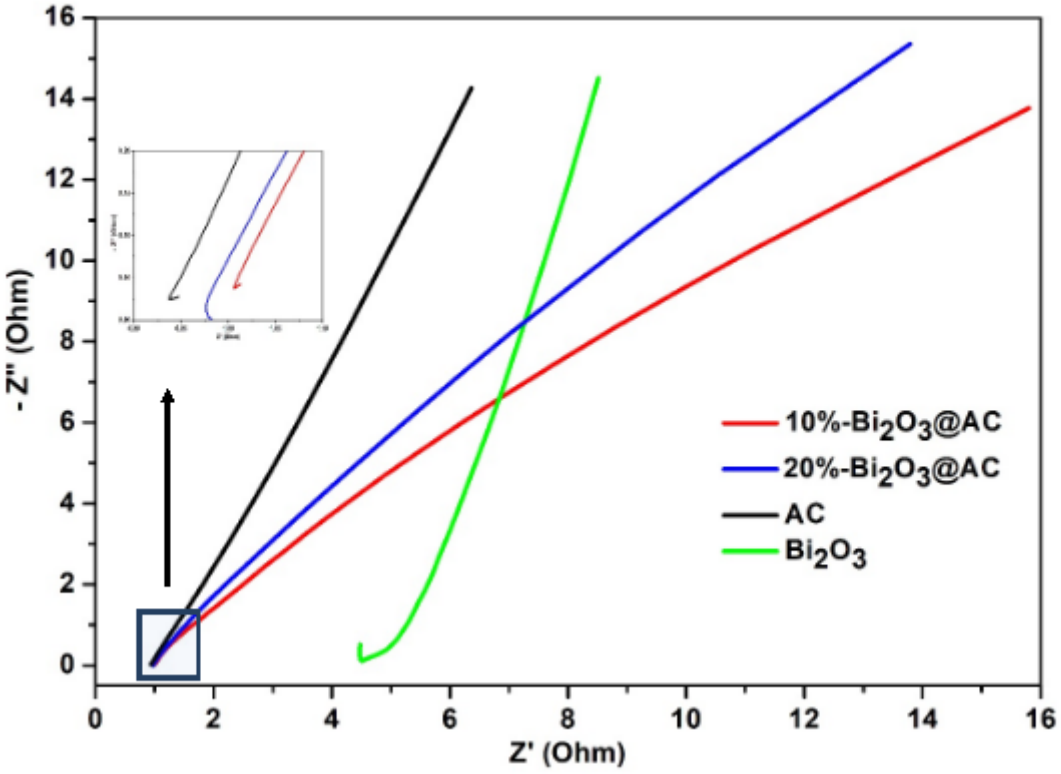

Figure 9

Nyquist plots of AC, commercial Bi2O3 and nanocomposites.